Ultra-sensitive graphene membranes for microphone applications

Supporting Information

Gabriele Baglioni,[*,†] Roberto Pezone,[‡] Sten Vollebregt,[‡] Katarina C. Zobenica,[¶] Marko Spasenovi´c,[¶] Dejan Todorovi´c,[§] Hanqing Liu,[‖] Gerard Verbiest,[‖] Herre S.J. van der Zant,[†] and Peter G. Steeneken[*,†,‖]

†*Kavli Institute of Nanoscience, TU Delft*

‡*Laboratory of Electronic Components, Technology and Materials, TU Delft* ¶*Center for Microelectronic Technologies, Institute of Chemistry, University of Belgrade*

§*Dirigent Acoustics Ltd, Belgrade, Serbia.*

‖*Department of Precision and Microsystems Engineering, TU Delft*

E-mail: G.Baglioni@tudelft.nl; P.G.Steeneken@tudelft.nl

S1. Raman and AFM

The crystallinity of the graphene is inspected by Raman spectroscopy using a Horiba HR800 spectrometer equipped with a 514.5 nm Ar+ laser maintained at 0.5 mW to limit possible degradation of the material. The objective used is 100x with a numerical aperture of 0.9, giving a spot size of about 696 nm. The Raman spectrum, shown in Fig. S1, is normalized to the amplitude of the G band. A total of twelve measurement points in the supported region (graphene on SiO2) show the three typical Raman bands that identify the graphene. The G-band and 2D-band are centred at ~ 1579.8 cm^{-1} and 2703.1 cm^{-1} with a $I_{2D}/I_G < 1$ that confirms its multi-layer nature[1,2] . The rise of the D-band at 1354.9 cm^{-1}, with $I_D/I_G < 0.2$,

shows the presence of defects in the material due to a locally distorted graphene lattice, like edges, vacancies, Stone-Wales defects, and wrinkles.

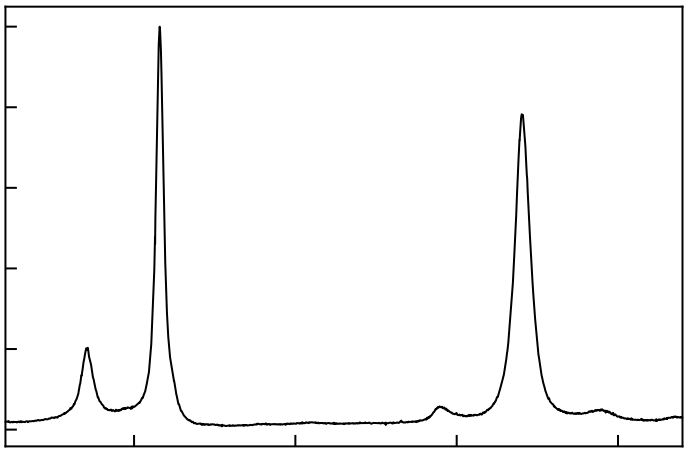

Figure S1: Raman spectrum. Raman spectrum of the CVD multilayer graphene.

We measured the graphene thickness with an atomic force microscope (AFM) from Cypher Asylum Research in semi-contact mode. Multiple profile scans of at the edge of the graphene sheet yield a thickness of ~ 7.7 ± 0.8 nm and are shown in Fig. S2.

S2. Additional data on mechanical sensitivity

Figure S3 shows the mechanical sensitivity at 1 kHz measured on all 37 graphene drums as well as the correlation between sensitivity and resonant frequency measured in atmospheric conditions.

a **b**

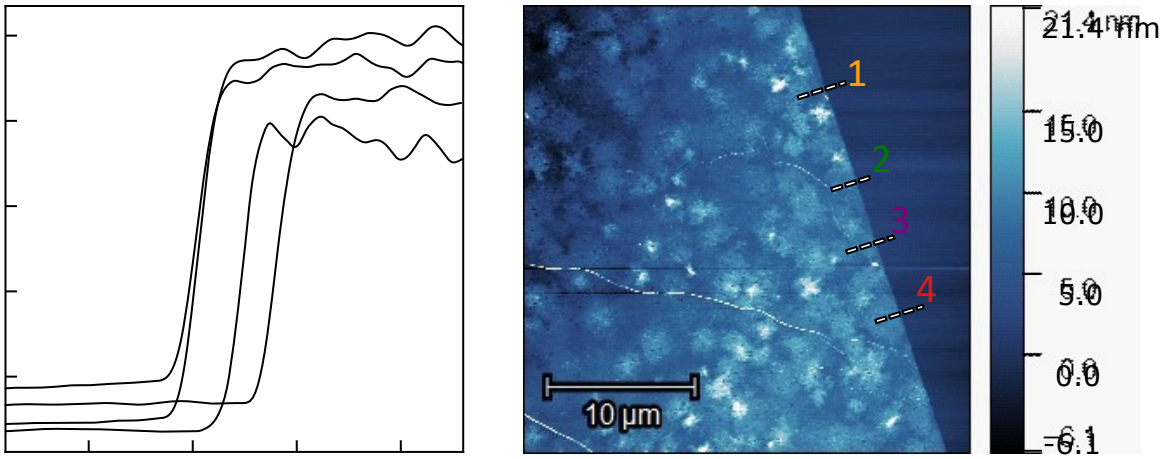

Figure S2: Thickness measurements.(a) Traces of AFM scans at the edge of the graphene sheet after transfer on the Si/SiO_2 substrate. (b) AFM map of the scanned area. The coloured lines highlight the regions where the step in Fig. S2a is measured.

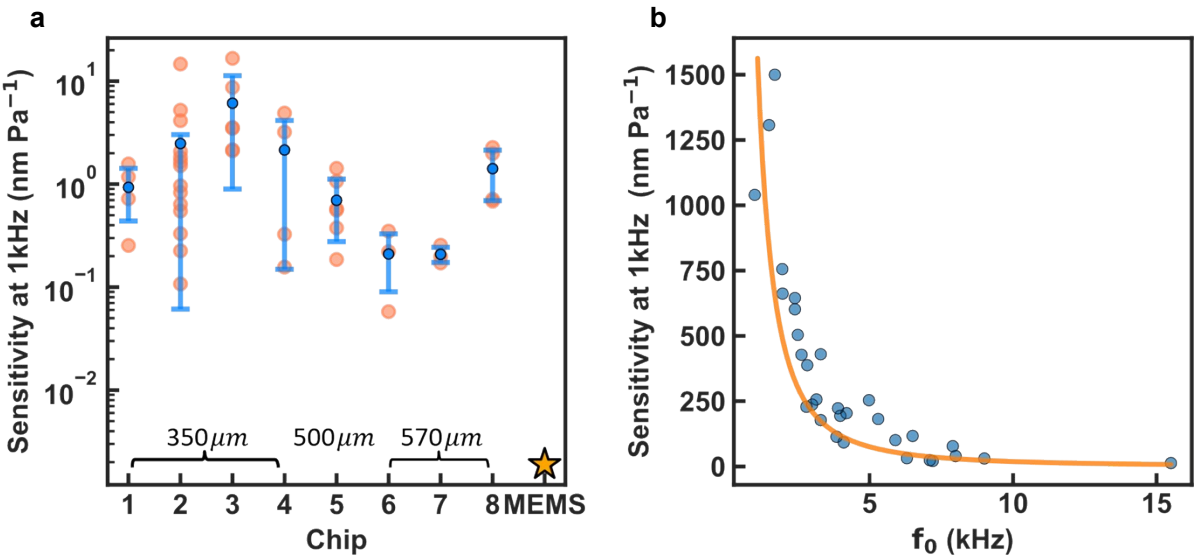

Figure S3: Mechanical sensitivity. a Mechanical sensitivities at 1 kHz of 37 graphene membranes on different chips. The performance varies significantly from sample to sample but all graphene membranes exhibit a higher sensitivity than the reference MEMS microphone. **b** Acoustic sensitivity of graphene membranes with d = 350μm at 1 kHz plotted against the fundamental resonant frequency f_0 measured in air from data like in Fig. 3a of the main text.

S3. Resonance frequency and air damping

Apart from detecting the resonance frequency in air using acoustic actuation, we also investigated the resonant response in vacuum using a scanning laser vibrometer from

Polytec. The sample was placed in a vacuum chamber (10^{-3} mbar) on a piezo-shaker used to actuate the mechanical resonance. The mechanical response was detected over a grid of points distributed over the surface of the membrane such that the mode shape at resonance could be reproduced. Figure S4a shows a typical spectrum with the resulting shape of first and second resonant mode for a membrane with d = 350μm. In table S1, we show the resonance frequency f_0 and Q-factor resulting from fit of curves in Fig. 3a of the main text (atmospheric conditions) as well as from fit to data like in Fig. S4 (vacuum condition 10^{-3} mbar). The origin of the different values for atmospheric and vacuum condition is not understood

yet.

Table S1: Resonance frequency and Q-factor of drums from Figure 3a. Resonance frequency and Q-factor resulting from fit of curves in Fig. 3a of the main text (atmospheric conditions), where drums are numbered from the top curve to bottom curve in Fig. 3a. Resonance frequency and Q-factor of same drums from fit to data like in Fig. S4 (vacuum condition 10^{-3} mbar).

Drum	f_0 (kHz)	Q	f_0 (kHz)	Q
1	1.5	1.1	14.4	161
2	2.6	1.6	21.4	254
3	4.6	1.5	22.7	268
4	6.7	3.1	33.5	236

A comparison between resonance frequencies measured in vacuum and air is shown in Fig. S4b. The observed ratio between resonance frequency in vacuum and in air is $f_{\text{vacuum}}/f_{\text{air}}$ ~ 5 – 10. The fundamental resonance frequency of a membrane can be expressed as $f_0 = \frac{2.405}{\pi R}\sqrt{\frac{n_0}{m_{\text{eff}}}}$. In atmospheric condition, the surrounding air is pushed along, adding mass to the resonator. In previous works[3,4] the membrane's effective mass is taken as

$$m_{\text{eff}} = \rho t\left(1 + \frac{2\rho_{\text{air}}R}{3\rho t}\right), \quad (1)$$

where ρ, t and R are the density, thickness and radius of the membrane and ρ_{air} is the density of air. As shown in Fig. S4b, Eq. 1 predicts a ratio f_{vacuum}/f_{air} of ~ 3.5 whereas the experimental ratio is higher, between 4-10. However, Eq. 1 was developed for valveless micropumps in the plate limit,[5] which can explain the disagreement between our measurement and Eq. 1. It might also be that the mass density of the graphene membrane ρt is lower than that of crystalline graphene. Further investigation is needed to better understand this effect on thin membranes dominated by in-plane pretension.

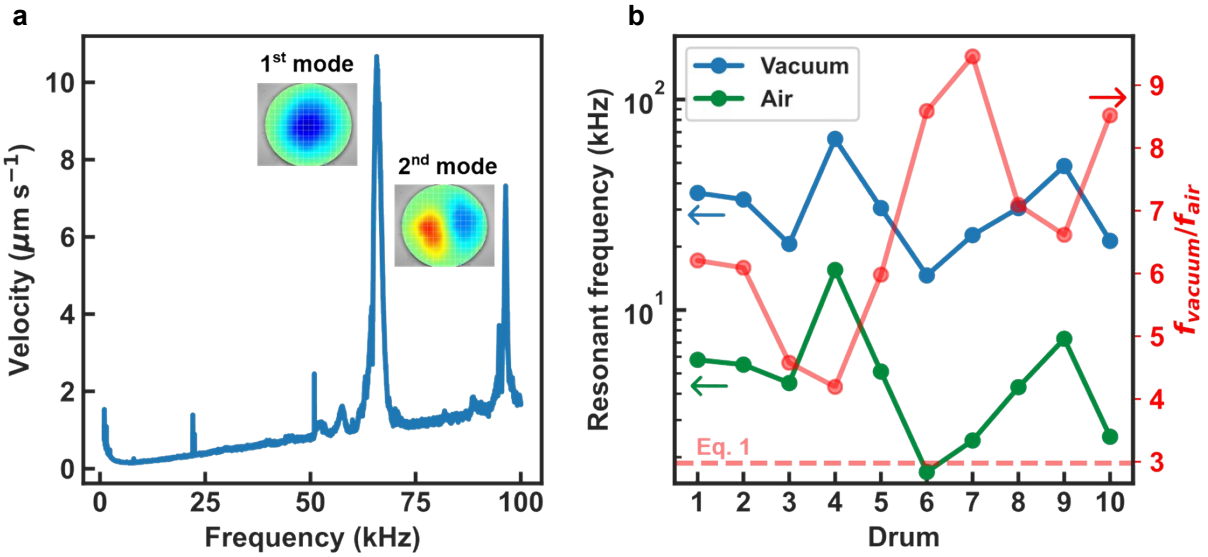

Figure S4: Resonance frequency: vacuum vs air (a) Mechanical spectra of a graphene membrane under piezoelectric actuation measured through a scanning laser vibrometer. Mode shapes corresponding to the first and second resonant peaks are also shown. (b) Comparison between resonance frequency measured in vacuum and in air (left y-axis) for different graphene drums. The ratio f_{vacuum}/f_{air} along with the expected value from Eq. 1 are also shown (right y-axis). Added air mass causes a significant decrease of the mechanical resonance frequency which is not well reproduced by theoretical model.

S4. Wrinkles

The sensitivity variation from sample to sample observed in Fig. 3b and S3 in the main manuscript was linked to the change in the membrane's pretension during the fabrication process. Moreover, wrinkles can form during the transfer process, introducing additional

non-uniformities in the strain over the surface of the membrane which can vary between different samples. This phenomenon can lead to deviations from the ideal deformation shape of a membrane as shown in Fig. S4a and thus different mechanical response from the membranes. In Fig S5, we show an example of two drums with different mode shape shapes arising from wrinkle-induced strain. The mode shapes were acquired with a digital holographic microscope (DHM) from Lynceetec paired with a laser pulsed stroboscopic unit. The measurements were carried out in vacuum conditions ($\sim 10^{-3}$ mbar) and the membranes were driven into resonance via piezoelectric actuation. The periodic signal driving the piezoshaker was controlled via the stroboscopic unit to synchronize excitation signal with the DHM laser pulse and camera shutter.

Videos of the recorded mode shapes of two membranes are also included as supplementary material to further illustrate possible wrinkle-induces deformation of the mode shapes.

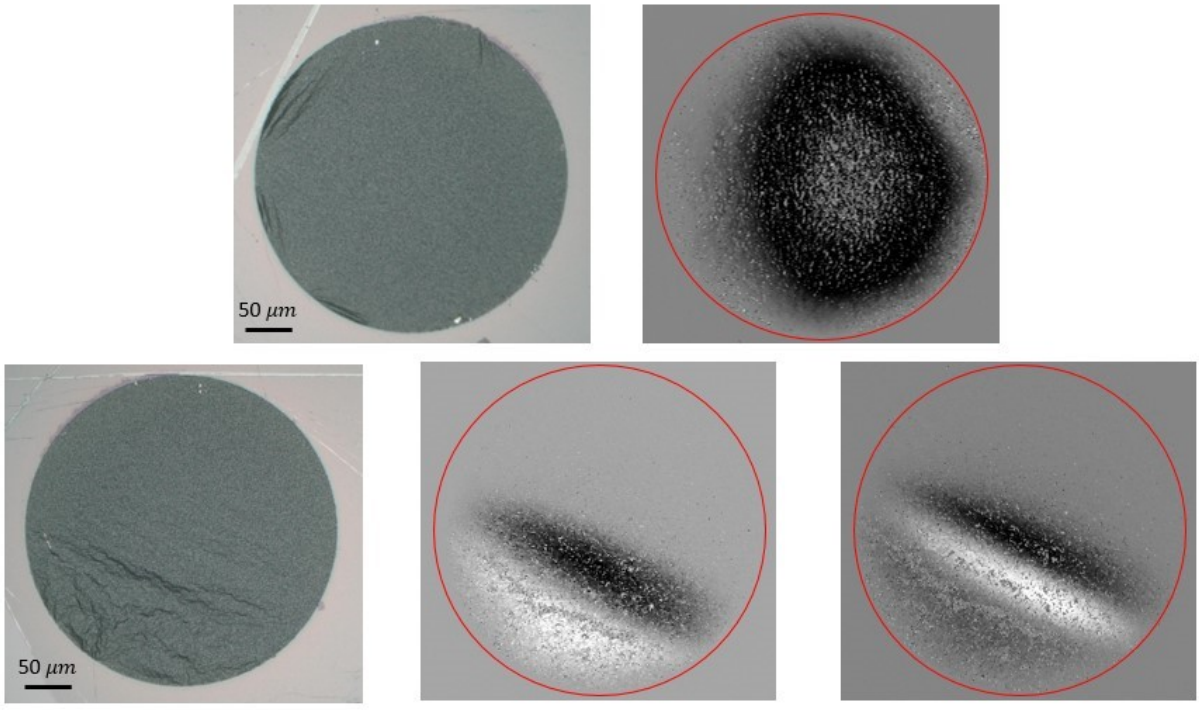

Figure S5: Wrinkles and drum deformation Examples of different deformation shapes on wrinkled graphene membranes measured with a stroboscopic technique in a DHM.

S5. SEM picture of graphene membranes

As mentioned in the main manuscript, small holes of < 50 nm are left on the graphene during the CVD growth. The SEM pictures on Fig. S6 show an example of these defects on a broken membrane. More samples have been inspected separately and their ML-gr morphology has the same type of defects with the same density as in Fig. S6

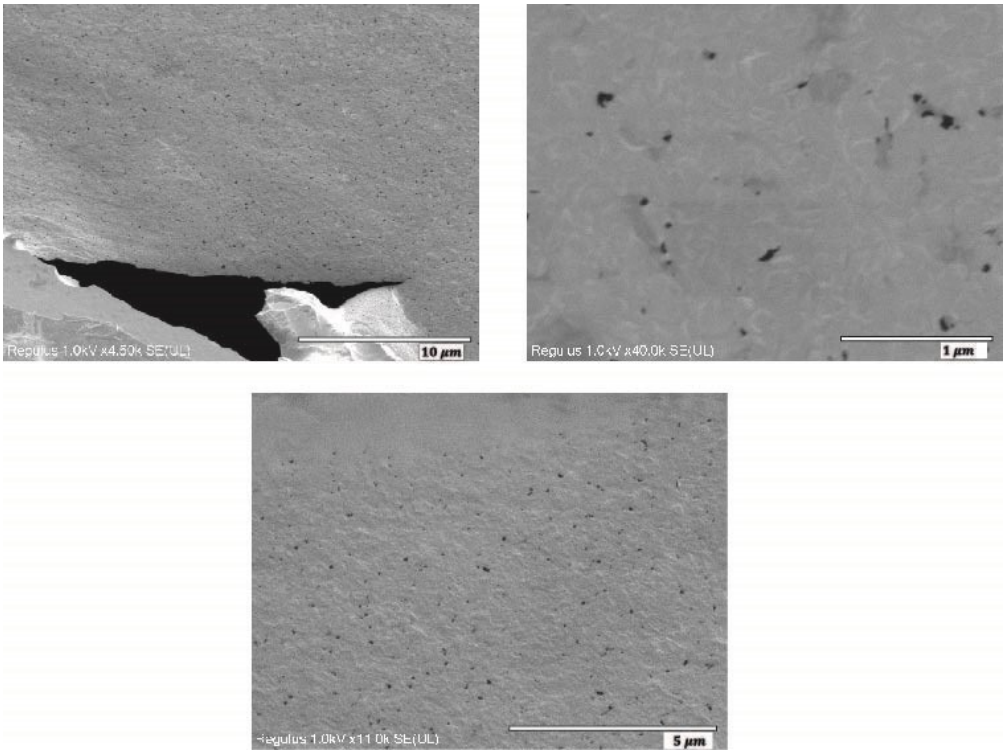

Figure S6: SEM pictures of suspended membrane SEM pictures of a broken suspended membrane showing small hole defects in the membrane.

S6. Bandwidth correction to mechanical compliance

As explained in the main text, we divided the mechanical compliances shown in Fig. 6 by the term $(20\ \text{kHz}/f_0)^2$ to account for differences in the resonance frequency, f_0, between the different devices. We do this because if the tension n_0 of the membranes would be increased by a factor $(20\ \text{kHz}/f_0)^2$ then their resonance frequency would increase by a factor

20 kHz/f_0 (since $f_0 \propto \sqrt{n_0}$), but their compliance would drop by a factor (20 kHz/f_0)^2 (since $C_m \propto n_0$). In Fig. S7 we plot the corrected values for the membrane in this work (orange hexagons), graphene membranes in literature reporting the membrane's resonance frequency (purple hexagons), MEMS devices from[6] (blue circles) and the commercial ST MEMS device (yellow star). The corrected values for the graphene membranes in this work are calculated from the data in Fig. S3. The datasheet for the ST MEMS[7] does not report explicitly the resonance frequency of the device but reports device performance only up to 10 kHz. We therefore assume that its resonance frequency is ≤ 20kHz and used a value of 20 kHz for this calculation. Thus, even after taking the difference in resonance frequency into account, the graphene membranes in this work exhibit higher compliance than most devices reported

in literature.

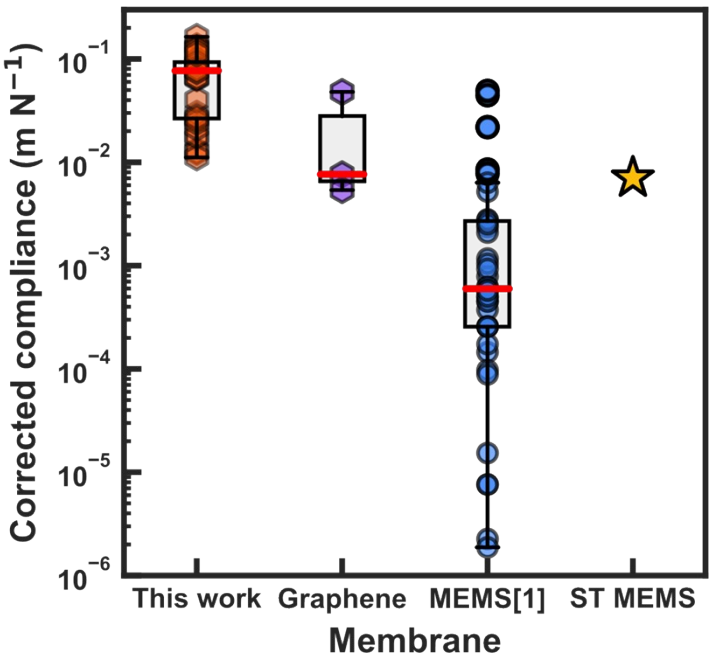

Figure S7: Corrected compliance Box plot of the mechanical compliance of membranes studied in this work normalized by (20 kHz/f_0)^2.

S7. Sound recording using the graphene membrane

In order to demonstrate the performance of the graphene membranes as microphones, we record a music soundtrack by optical readout of the graphene motion. The output signal from the vibrometer in response to sound was measured with a sampling frequency of 20 kHz. The recorded waveform was converted back to an audio file which is included as supporting material.

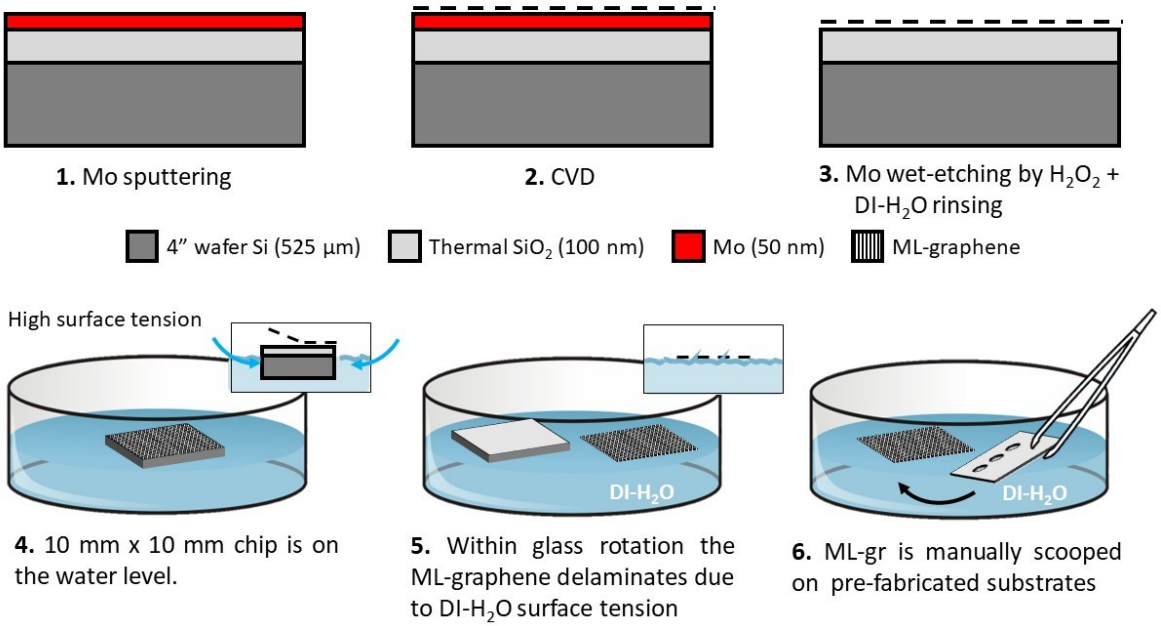

Figure S8: Growth and transfer processes of the graphene membranes.

S8. Growth and transfer processes

The graphene growth synthesis is detailed in previous work.[8] For this work, the 4" wafer with Mo is heated at around 905 °C in H2 (1000 sccm) and Ar (500 sccm) environment for 1200 s to reduce the oxidized surface (annealing step at 25 mbar). Then, a growth step at same pressure of 1200 s at around 935 °C with CH_4 (25 sccm), H_2 (40 sccm), and Ar (960

sccm) gas flows is performed. A final cooling step under Ar atmosphere is done. The entire transfer steps are shown in the supplementary Figure S8.

References

(1) Malard, L. M.; Pimenta, M. A.; Dresselhaus, G.; Dresselhaus, M. S. Raman spectroscopy in graphene. *Physics Reports* **2009**, *473*, 51–87.

(2) Pimenta, M. A.; Dresselhaus, G.; Dresselhaus, M. S.; Canc¸ado, L. G.; Jorio, A.; Saito, R. Studying disorder in graphite-based systems by Raman spectroscopy. *Physical Chemistry Chemical Physics* **2007**, *9*, 1276–1290.

(3) Al-mashaal, A. K.; Wood, G. S.; Torin, A.; Mastropaolo, E.; Newton, M. J.; Cheung, R. Dynamic behavior of ultra large graphene-based membranes using electrothermal transduction. *Applied Physics Letters* **2017**, *111*, 243503.

(4) Xu, J.; Wood, G. S.; Mastropaolo, E.; Newton, M. J.; Cheung, R. Realization of a Graphene/PMMA Acoustic Capacitive Sensor Released by Silicon Dioxide Sacrificial Layer. *ACS Applied Materials & Interfaces* **2021**, *13*, 38792–38798.

(5) Pan, L. S.; Ng, T. Y.; Wu, X. H.; Lee, H. P. Analysis of valveless micropumps with inertial effects. *Journal of Micromechanics and Microengineering* **2003**, *13*, 390–399.

(6) Zawawi, S. A.; Hamzah, A. A.; Majlis, B. Y.; Mohd-Yasin, F. A Review of MEMS Capacitive Microphones. *Micromachines* **2020**, *11*, 484.

(7) STMicroelectronics, MP23DB01HP Datasheet MEMS audio sensor: digital microphone with multiple performance modes. **2021**,

(8) Grachova, Y.; Vollebregt, S.; Lacaita, A. L.; Sarro, P. M. High Quality Wafer-scale CVD Graphene on Molybdenum Thin Film for Sensing Application. *Procedia Engineering* **2014**, *87*, 1501–1504, EUROSENSORS 2014, the 28th European Conference on Solid-State Transducers.